Chinese Journal of Chemistry, **2004**, *22*, 792—797

Article

Quantum Chemical Study on Reaction of Acetaldehyde with Hydroxyl Radical

LI, Ming*(李明) ZHANG, Jin-Sheng(张金生)
SHEN, Wei(申伟) MENG, Qing-Xi(孟庆喜)

Department of Chemistry, Southwest-China Normal University, Chongqing 400715, China

The reaction of acetaldehyde with hydroxyl radical was studied by means of quantum chemical methods. The geometries for all the stationary points on the potential energy surfaces were optimized fully, respectively, at the G3MP2, G3, and MP2/6-311＋＋G(d,p) levels. Single-point energies of all the species were calculated at the QCISD/6-311＋＋G(d,p) level. The mechanism of the reaction studied was confirmed. The predicted product is acetyl radical that is in agreement with the experiment.

Keywords hydroxyl radical, acetaldehyde, mechanism, quantum chemical study

Introduction

Peroxyacetyl nitrate (PAN), as a kind of continuous pollution products, is formed by the combination reaction of acetaldehyde and nitric oxide in the photochemical smog. All the chemical substances that can lead to acetaldehyde and acetyl radical may be the source of PAN.[1] The atmospheric degradation of CH_3CHO occurs by its reaction with OH radical,[2] or by photodissociation.[3] While CH_3CHO reacts with OH radical, it is assumed to produce CH_3CO radical that may react with O_2 to form acetyperoxy radical, $CH_3C(O)O_2$, and further combine with NO_2 into PAN.[4] By means of the method of pulsed laser photolysis combined with direct detection by transient absorption spectroscopy and resonance fluorescence, Cameron, *et al.*,[5] quantified the primary products in the reaction between CH_3CHO and OH. The following reactions presumed are :

$$HO + CH_3CH \rightarrow H + CH_3COOH \quad (a)$$

$$\rightarrow CH_3 + HCOOH \quad (b)$$

$$\rightarrow H_2O + CH_2CHO \quad (c)$$

$$\rightarrow H_2O + CH_3CO \quad (d)$$

Vandenberk, *et al.*,[6] found the reaction (d) at room temperature. There were some reports about the reaction enthalpies, $\Delta_r H_{298}$, for the reactions (a), (b), (c), and (d)[7] and the rate coefficient for the reaction (d).[8-13] Aloiso, *et al.*,[14] studied the structures of the $HOCH_3CHO$ complexes at the B3LYP/6-311＋＋G(3df,3pd) level. Alvarez-Idaboy, *et al.*,[15] investigated the intermediates and the transition states for the reaction (d) at the MP2/6-311＋＋G(d,p) level. However, the systemic mechanism of this reaction has not been discussed in detail theoretically. In the present paper, therefore, the mechanism of the reaction of acetaldehyde with hydroxyl radical is predicted by means of quantum chemical methods.

Computational methods

The reaction of CH_3CHO with OH was studied by means of quantum chemical methods G3MP2, G3, MP2, and QCISD. The geometries of reactants (**Re**), intermediates (**M**), transition states (**T**), and products (**P**) were optimized fully, respectively, at the G3MP2, G3, and MP2/6-311＋＋G(d,p) levels. The vibrational frequencies and zero-point energies (ZPE) of all the optimized structures were calculated at the MP2/6-311＋＋G(d,p) level. Also, single-point energies were obtained at the QCISD/6-311＋＋G(d,p) level. With the wave functions obtained from MP2/6-311＋＋G(d,p) level, the electron densities at the bond critical points (BCP) for the optimized structures were calculated by means of the AIM2000 program package.[16] The BCP is a saddle point at the electron density, ρ, and appears between any two nuclei bonded chemically. At the BCP, $\nabla\rho=0$. The magnitude of the electron density at the BCP is indicative of the strength of the bond.[17,18] All the transition states were verified by internal reaction coordinate (IRC) calculation of the optimized structures obtained at the MP2/6-311＋＋G(d,p) level. All calculations were performed with the program GAUSSIAN 03.[19]

Results and discussion

All the the stationary points on the potential energy

* E-mail: liming@swnu.edu.cn
Received November 24, 2003; revised February 23, 2003; accepted April 6, 2003.
Project supported by the Natural Science Foundation of Chongqing of China (No. 2002-7473).

surfaces (PES) were positively identified for local minima with zero of the number of imaginary frequencies and for transition states with one. The transition states were verified by the IRC calculation at the MP2/6-311++G(d,p) level. As shown, there are six channels for the reaction between CH_3CHO and OH. These channels lead to the products H+CH_3COOH (**P1**), CH_3+HCOOH (**P2**), H_2O+CH_3CO (**P3**) and H_2O+CH_2CHO (**P4**):

Re→T5→P4 (1)

Re→M1→T4→P3 (2)

Re→M1→T1a→M2a→T2a→P1 (3)

Re→M1→T1b→M2b→T2b→P1 (4)

Re→M1→T1a→M2a→T3a→P2 (5)

Re→M1→T1b→M2b→T3b→P2 (6)

The equilibrium geometries of all the stationary points optimized at the MP2/6-311++G(d,p) level are illustrated in Figure 1. Two-dimensional electron density contours for all the species are presented in Figure 2. The reaction energy relationship obtained at the QCISD/6-311++G(d,p) level is demonstrated in Figure 3. Relative energies, forward reaction barriers, $\Delta E^{\neq}$, and selected vibrational frequencies for various species are summarized in Table 1. For comparison, the calculated reaction enthalpies $\Delta_r H_{298}$ and the available experimental data[7] are listed in Table 2. In the following discussion, all the energies were obtained from the QCISD/6-311++G(d,p) calculation of the structures optimized at the MP2/6-311++G(d,p) level.

Table 2 Reaction enthalpies $\Delta_r H_{298}$/(kJ•mol^{-1})

	G3MP2	G3	MP2 6-311++G(d,p)	Expt[7]
Re	0	0	0	0
P1	−80.0	−82.8	−108.4	−87
P2	−86.3	−88.6	−91.2	−106
P3	−119.8	−119.5	−131.9	−125
P4	−93.5	−94.4	−69.5	−104

Formation of H and CH_3COOH

There are two reaction paths leading to the products H and CH_3COOH. Through the hydrogen-bond between the H(1) and the O(5), the reaction of CH_3CHO with OH leads to the intermediate **M1**. **M1** is of C_s symmetry and may be attacked by the O(2) from two different sides to form the transition states **T1a** and **T1b**, which generate the intermediates **M2a** and **M2b** respectively. Further, the products H and CH_3COOH are generated with the reaction through the transition states **T2a** and **T2b**. Since **T1b**, **M2b**, and **T2b** are, respectively, the enantiomers of **T1a**, **M2a**, and **T2a**, the species discussed in the following are **T1a**, **M2a**, and **T2a**.

As shown, the H(1), O(2), H(3), C(4), O(5), C(6), and H(7) atoms of **M1** close to coplanarity. The O(2)-H(1)-O(5), H(1)-O(5)-C(4), and O(5)-C(4)-H(3) angles are 166.4°, 113.1°, and 119.8° respectively (Figure 1). The H(1)—O(5) distance is 0.1940 nm and the corresponding Mülliken overlap population is 0.04. The electron density at the bond critical point (BCP) of the H(1)—O(5) bond is 0.0227 (Figure 2), which shows the

Table 1 Relative energies (kJ/mol), forward reaction barriers $\Delta E^{\neq}$ (kJ/mol), and vibrational frequencies ν (cm^{-1}) for various species in the HO+CH_3CHO reaction

Species	G3MP2	MP2 6-311++G(d,p)+ZPE	G3	QCISD 6-311++G(d,p)	$\Delta E^{\neq}$	Vibrational frequencies	
						ν_1	ν_2
Re	0	0	0	0			
M1	−16.02	−17.59	−17.59	−23.63		38.1	54.2
T1a	20.22	66.16	16.54	29.14	52.77	862.0i	216.2
T1b	20.22	66.16	16.54	29.14	52.77	862.1i	216.2
M2a	−73.78	−55.66	−76.40	−81.65		229.2	295.2
M2b	−73.78	−55.66	−76.40	−81.65		229.2	295.2
T2a	−16.28	18.90	−19.17	17.59	99.24	1785.5i	240.7
T2b	−16.28	18.90	−19.17	17.59	99.24	1785.5i	240.7
P1	−80.08	−107.65	−82.97	−55.92			
T3a	−44.37	−13.39	−47.52	−26.78	54.87	773.0i	202.5
T3b	−44.37	−13.39	−47.52	−26.78	54.87	773.0i	202.5
P2	−86.38	−91.63	−88.74	−68.79			
T4	−10.76	12.08	−14.44	2.10	25.73	1066.3i	71.6
P3	−119.99	−133.11	−119.72	−113.16			
T5	14.70	27.83	11.81	34.39	34.39	2151.6i	70.9
P4	−93.73	−70.10	−94.52	−77.19			

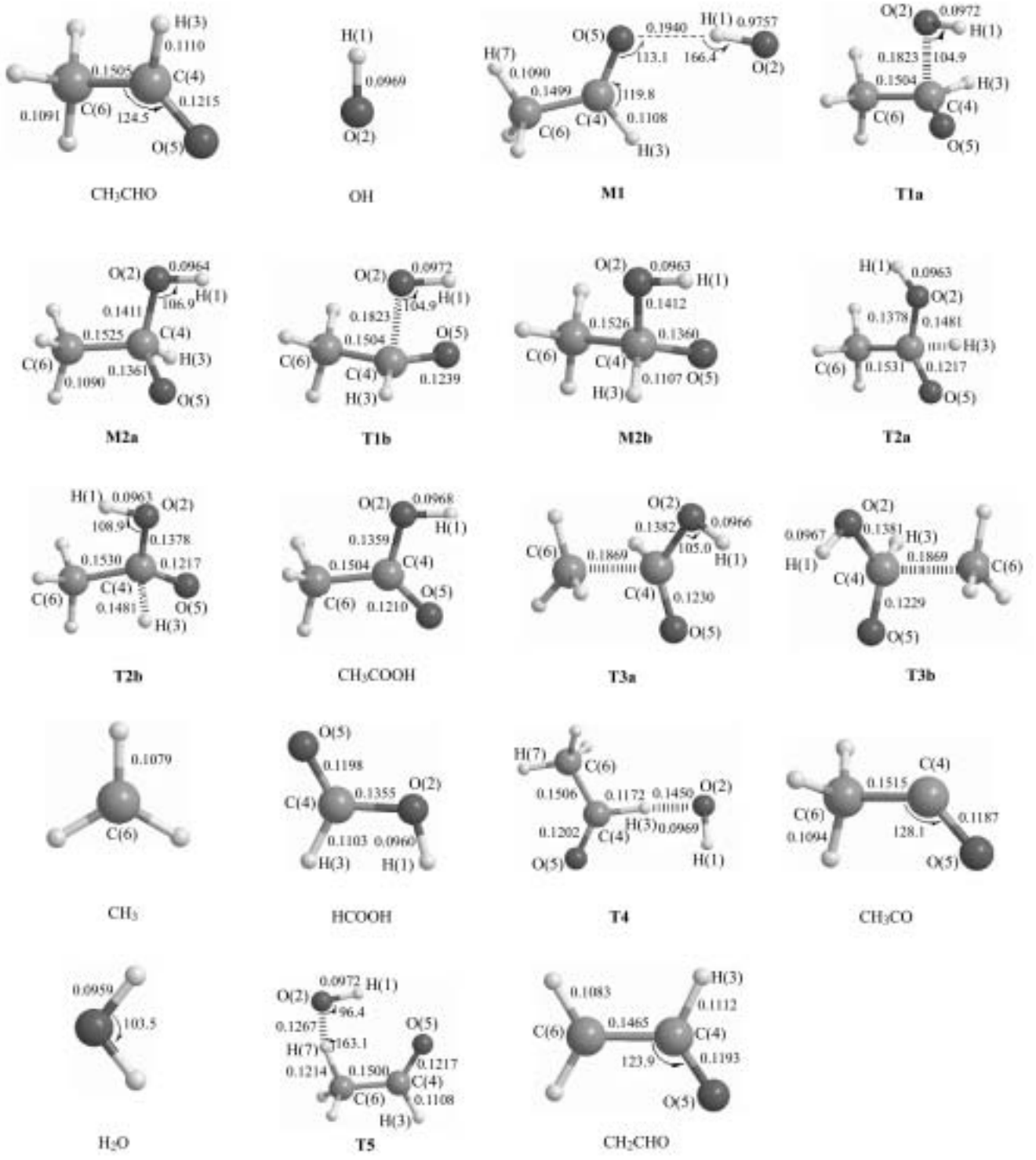

Figure 1 Optimized structures of all the species for the reaction of CH_3CHO with OH radical at the MP2/6-311++G(d,p) level (bond lengths in nm, bond angles in degree).

interaction between the H(1) and the O(5). The C(4)—O(5) bond is 0.1220 nm and longer than the carbonyl bond in CH_3CHO (0.1215 nm). As presented in Table 1, the energy of **M1** is lower than that of reactants by 23.63 kJ/mol. In the transition state **T1a**, the H(1)-O(2)-C(4) and O(2)-C(4)-C(6) angles are 104.9° and 100.7°, respectively. The O(2)—C(4) distance is 0.1823 nm and its Mülliken overlap population is 0.08 and its electron density at the BCP is 0.0935, which illustrate the noticed interaction between the O(2) and the C(4) of **T1a**. The intermediate **M2a** is formed with the reaction through the transition state **T1a**. The O(2)—C(4) bond of **M2a** is 0.1411 nm. The energy of **M2a** is lower than that of **T1a** by 110.80 kJ/mol. The increase in the H(3)—C(4) distance of **M2a** leads to the transition state **T2a**. As illustrated in Figure 1, the H(3)—C(4) distance

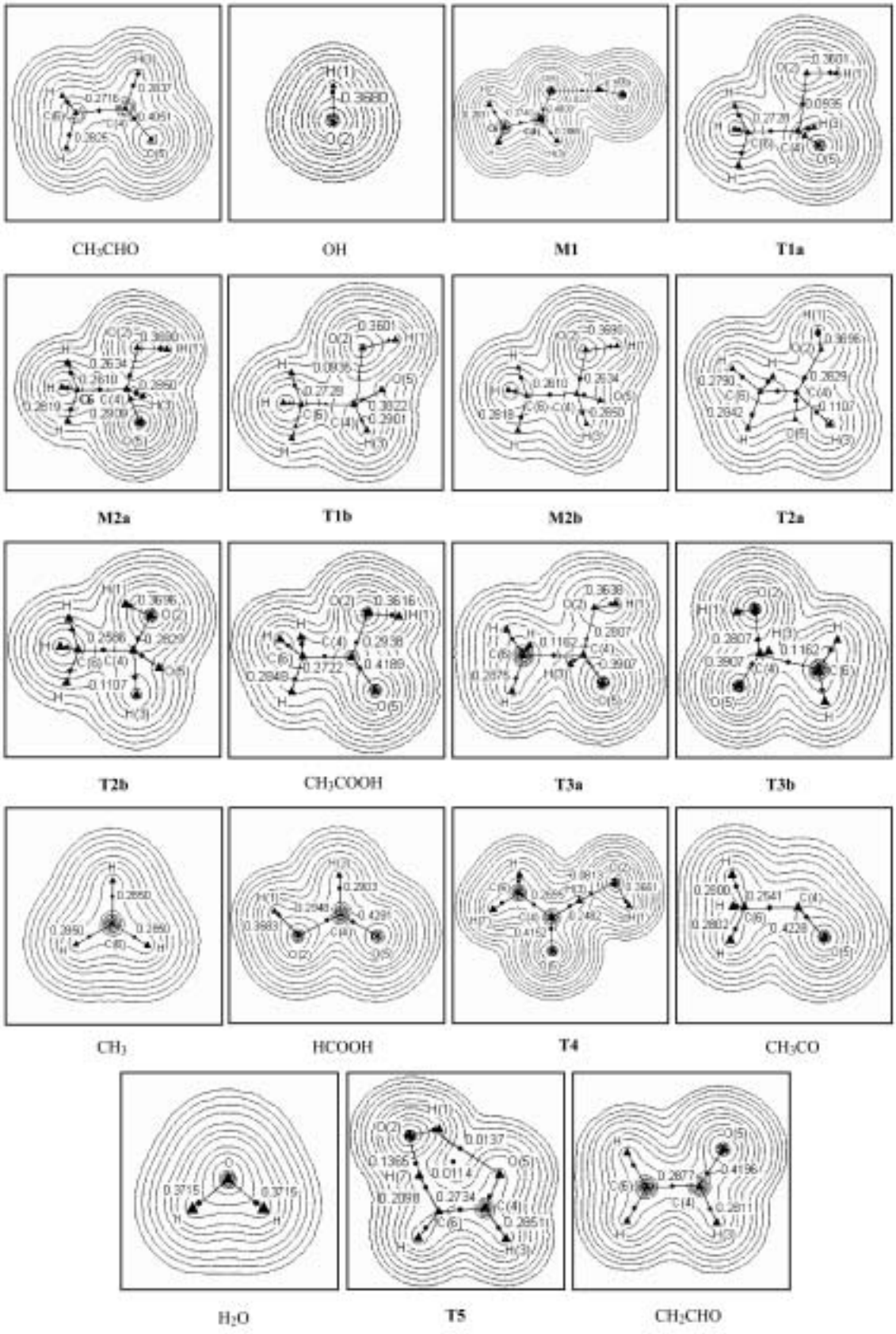

Figure 2 Two-dimensional electron density contours for all species at the MP2/6-311＋＋G(d,p) level (including electron densities at some selected BCPs).

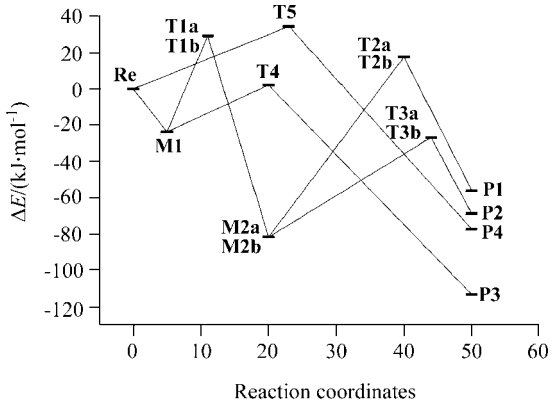

Figure 3 Energy relationship for the reaction of CH_3CHO with OH radical at the QCISD/6-311++G(d,p) level.

of **T2a** is 0.1481 nm. Its Mulliken overlap population (0.14) and its electron density at the BCP (0.1107) are much less than those of **M2a** (0.42 and 0.2850). Finally, the fracture of the H(3)—C(4) bond of **T2a** leads to the products H and CH_3COOH.

As demonstrated in Table 1, the reaction leading to the product **P1** is exothermic and its released heat quantity is 55.92 kJ/mol. The forward reaction barriers between **M1** and **T1a** and between **M2a** and **T2a** are, respectively, 52.77 kJ/mol and 99.24 kJ/mol. It is clear that the decomposition of **M2a** into the product **P1** via **T2a** is the rate controlling step for this reaction channel.

Formation of CH_3 and HCOOH

There are also two reaction channels leading to the products CH_3 and HCOOH. These reaction channels go through formation of **M1**, **M2a**, and **M2b**. With the C(4)—C(6) distances of **M2a** and **M2b** increasing, the transition states **T3a** and **T3b** are formed. Finally, the fracture of the C(4)—C(6) bonds of **T3a** and **T3b** leads to CH_3 and HCOOH. **T3a** and **T3b** are enantiomers. The C(4)—C(6) bonds of **T3a** and **T3b** are 0.1869 nm and their Mülliken overlap populations are 0.13. Their electron densities at the BCP are 0.0216. Obviously, the C(4)—C(6) bonds are weakened greatly. The forward reaction barrier between **M2a** (or **M2b**) and **T3a** (or **T3b**) are 54.87 kJ/mol and higher than 52.77 kJ/mol between **M1** and **T1a**. The released heat quantities for these reaction channels are 68.79 kJ/mol.

Formation of H_2O and CH_3CO

The attack of the O(2) of the intermediate **M1** on the H(3) and the fracture of the H(1)—O(5) bond lead to the transition state **T4**. The optimized structure of **T4** is shown in Figure 1. The H(1), O(2), H(3), C(4), O(5), C(6), and H(7) atoms are nearly coplanar. The H(1)—O(2), O(2)—H(3), and H(3)—C(4) bonds are, respectively, 0.0969, 0.1450, and 0.1172 nm. The H(1)-O(2)-H(3) and O(2)-H(3)-C(4) angles are 94.3° and 175.0°. The electron density at the BCP of the H(3)—C(4) bond of **T4** is 0.2482 and smaller than 0.2866 of **M1**. Therefore, the H(3)—C(4) bond is weakened. The electron density at the BCP of the O(2)—H(3) bond is 0.0813, which shows the noticed interaction between O(2) and H(3). Further, the fracture of the H(3)—C(4) bond of **T4** leads to the products H_2O and CH_3CO. As illustrated in Table 1, the forward reaction barrier between **M1** and **T4** is 25.73 kJ/mol and the released heat quantity for this reaction channel is 113.16 kJ/mol.

Formation of H_2O and CH_2CHO

The attack of the O atom of the OH radical on the H atom of methyl of CH_3CHO leads to the transition state **T5**. The products H_2O and CH_2CHO are generated via the transition state **T5**. The H(1), O(2), H(7), C(6), C(4), O(5), and H(3) atoms of **T5** are nearly coplanar. The H(1)—O(2), O(2)—H(7), C(6)—H(7), C(4)—C(6), and C(4)—O(5) bonds are illustrated in Figure 1 and their electron densities at the BCPs are shown in Figure 2. As demonstrated, the C(6)—H(7) bond of **T5** is weakened and its bond length (0.1214 nm) is much longer than the normal C—H bond. In despite of a long H(1)—O(5) bond (0.2250 nm), its Mulliken overlap population and its electron density at the BCP are, respectively, 0.01 and 0.0137, which imply the interaction between H(1) and O(5). In addition, a ring critical point (RCP) with 0.0114 of electron density is found in the center of the H(1)-O(2)-H(7)-C(6)-C(4)-O(5) plane and this may imply the formation of a six-membered ring. As shown in Table 1, the forward reaction barrier between **Re** and **T5** is 34.39 kJ/mol. The fracture of the H(7)—C(6) bond of **T5** generates the products H_2O and CH_2CHO. The released heat quantity for this reaction channel is 77.19 kJ/mol.

It is clear from above discussion that the forward reaction barriers of rate controlling steps are 99.24, 99.24, 54.87, 54.87, 25.73, and 34.39 kJ/mol for six channels of the reaction of CH_3CHO with OH, respectively. Obviously, the reaction channel leading to the CH_3CO radical is the most favorable and the next is the channel generating the CH_2CHO radical. The theoretical estimation is in agreement with the experiment. All the reaction channels are exothermic. In addition, the calculated reaction enthalpies are in agreement with the experimental data (in Table 2). The energy relationship for the reaction of CH_3CHO with OH calculated at the QCISD/6-311++G(d,p) level is demonstrated in Figure 3.

Conclusion

In summary, there are six channels for the reaction of acetaldehyde with hydroxyl radical and every channel is exothermic. The most favorable product is the CH_3CO radical, which is in agreement with the experiment.

References

1 Roberts, J. M. *Atmos. Environ., Part A* **1990**, *24*, 243.
2 Kerr, J. A.; Sheppard, D. W. *Environ. Sci. Technol.* **1981**, *15*, 960.

3 Horowitz, A.; Calvert, J. G. *J. Phys. Chem.* **1982**, *86*, 3105.
4 Bridier, I.; Caralp, F.; Loirat, H.; Lesclaux, R.; Veyret, B.; Becker, K. H.; Reimer, A.; Zabel, F. *J. Phys. Chem.* **1991**, *95*, 3594.
5 Cameron, M.; Sivakumaran, V.; Dillon, T. J.; Crowley, J. N. *Phys. Chem. Chem. Phys.* **2002**, *4*, 3628.
6 Vandenberk, S.; Peeters, J. *J. Photochem. Photobiol., A Chem.* **2003**, *157*, 269.
7 Atkinson, R.; Baulch, D. L.; Cox, R. A.; Hampson, R. F. J.; Kerr, J. A.; Rossi, M. J.; Troe, J. *J. Phys. Chem. Ref. Data* **2000**, *29*, 167.
8 Atkinson, R.; Baulch, D. L.; Cox, R. A.; Hampson, R. F. J.; Kerr, J. A.; M. J. Rossi, M. J.; Troe, J. *J. Phys. Chem. Ref. Data* **1997**, 26, 1329.
9 Finlayson-Pitts, B. J.; Pitts, N. *Atmospheric Chemistry*: *Fundamentals and Experimental Techniques*, Wiley-Interscience, New York, **1986**.
10 Mallard, W. G.; Westley, F.; Herron, J. T.; Hampson, R. F.; Frizzell, D. H. *The NIST Chemical Kinetics Data Base*, *NIST Standard Reference Database*, Department of Commerce, Technology Administration, National Institute of Standards and Technology, Gaithersburg, United States, **1998**, 17-2Q98.
11 Butkovskaya, N. I.; Setser, D. W. *J. Phys. Chem. A* **2000**, *104*, 9428.
12 Morris, E. D.; Stedman, Jr. D. H.; Niki, H. *J. Am. Chem. Soc.* **1971**, *93*, 3570.
13 Balestra-Garcia, C.; Bras, G. L.; Leod, H. M. *J. Phys. Chem.* **1992**, *96*, 3312.
14 Aloiso, S.; Francisco, J. S. *J. Phys. Chem. A* **2000**, *104*, 3211.
15 Alvarez-Idaboy, J. R.; Mora-Diez, N.; Boyd, R. J.; Vivier-Bunge, A. *J. Am. Chem. Soc.* **2001**, *123*, 2018.
16 *AIM2000*, Version 1, Biegler-könig, F.; Schönbohm, J.; Derdau, R.; Bayles, D.; Bader, R. F. W., Midstream, Incorporation, San Brunno, U.S.A., **2000**.
17 Bader, R. F. W. *Atoms in Molecules-A Quantum Theory*, Oxford University Press, Oxford, **1990**.
18 Bader, R. F. W.; Popelier, P. L. A.; Keith, T. A. *Angew. Chem., Int. Ed. Engl.* **1994**, *33*, 620.
19 *Gaussian 03, Revision A.1*, Frisch, M. J.; Trucks, G. W.; Schlegel, H. B.; Scuseria, G. E.; Robb, M. A.; Cheeseman, J. R.; Montgomery, J. A.; Vreven, Jr. T.; Kudin, K. N.; Burant, J. C.; Millam, J. M.; Iyengar, S. S.; Tomasi, J.; Barone, V.; Mennucci, B.; Cossi, M.; Scalmani, G.; Rega, N.; Petersson, G. A.; Nakatsuji, H.; Hada, M.; Ehara, M.; Toyota, K.; Fukuda, R.; Hasegawa, J.; Ishida, M.; Nakajima, T.; Honda, Y.; Kitao, O.; Nakai, H.; Klene, M.; Li, X.; Knox, J. E.; Hratchian, H. P.; Cross, J. B.; Adamo, C.; Jaramillo, J.; Gomperts, R.; Stratmann, R. E.; Yazyev, O.; Austin, A. J.; Cammi, R.; Pomelli, C.; Ochterski, J. W.; Ayala, P. Y.; Morokuma, K.; Voth, G. A.; Salvador, P.; Dannenberg, J. J.; Zakrzewski, V. G.; Dapprich, S.; Daniels, A. D.; Strain, M. C.; Farkas, O.; Malick, D. K.; Rabuck, A. D.; Raghavachari, K.; Foresman, J. B.; Ortiz, J. V.; Cui, Q.; Baboul, A. G.; Clifford, S.; Cioslowski, J.; Stefanov, B. B.; Liu, G.; Liashenko, A.; Piskorz, P.; Komaromi, I.; Martin, R. L.; Fox, D. J.; Keith, T.; Al-Laham, M. A.; Peng, C. Y.; Nanayakkara, A.; Challacombe, M.; Gill, P. M. W.; Johnson, B.; Chen, W.; Wong, M. W.; Gonzalez, C.; Pople, A., Gaussian Inc., Pittsburgh PA, **2003**.

(E0311243 SONG, J. P.)